Quantum Chemical Simulations of the Proton Transfer in Water Wires Attached to Molecular Walls

Alexander V. Nemukhin,*,† Bella L. Grigorenko,† Igor A. Topol,*,‡ and Stanley K. Burt‡

Chemistry Department, M.V. Lomonosov Moscow State University, Moscow 119899, Russian Federation, and Advanced Biomedical Computing Center, SAIC Frederick, National Cancer Institute at Frederick, P.O. Box B, Frederick, Maryland 21702

Received: October 23, 2002; In Final Form: February 4, 2003

Quantum chemical methods are applied to study the stages of the proton transfer in water wires attached to molecular walls containing the side chains of His and Asp residues. Several molecular models of variable complexity are considered by using different techniques, and in every case, the most important reactions of cleavage and formation of chemical bonds in proton wires are treated at the ab initio level. The largest molecular model, which mimics structural elements of the M2 ion channel, is investigated with the help of a quantum mechanical−molecular mechanical (QM/MM) method with flexible effective fragments. Smaller models are considered at nonempirical levels in order to purify conclusions of the QM/MM approach. The results of calculations show that the only transition state structure found on the proton-transfer route refers to the stage of proton detachment from the N_ϵ atom of the imidazole ring to the neighboring water molecule. The corresponding energy barriers are estimated.

1. Introduction

Proton transfer processes across chains of donors and acceptors play an important role in chemistry and biology. A number of theoretical studies of proton transfer in isolated or solvated hydrogen-bonded clusters have been described in recent years. In most of these simulations, short chains of hydrogen-bonded molecules with an excess proton are analyzed, in many cases, by imposing restraints on the model molecular system in order to keep the quasilinear shape of the wire. Some of these calculations used empirical or empirically adjusted potentials, for example, refs 1 and 2. Many of them are based on the original or modified empirical valence bond (EVB) approach of Warshel and coauthors,[3,4] in particular, refs 5−8, others considered quantum dynamical approaches,[9,10] or the quantum mechanical−molecular mechanical (QM/MM)[11] type calculations.[12,13] Very interesting are the approaches to model water wires directly in ion channels by considering the molecular structure of the latter. Sagnella, Laasonen, and Klein [14] carried out Car-Parrinello molecular dynamics (MD) simulations for the $(H_2O)_5H^+$ cluster embedded into a polyglycine channel consisting of 13 Gly residues twisted into a 10 Å right-handed β-helix. It was found that a transient $H_5O_2^+$ complex is readily formed inside the channel. Another important conclusion of this work was that there existed a correlation between the carbonyl−oxygen solvation of the hydronium's nearest-neighbor water and the proton-transfer event. In the recent paper of Pomès and Roux,[15] the classical MD simulations are described for the system composed of a polypeptide gramicidin channel, a chain of 10 water molecules inserted inside the channel, and two cylindrical caps of water molecules lying outside the mouths of the channel. The CHARMM force field was used for protein−protein interactions, whereas the water wire was modeled with the empirical force field of Stillinger and co-workers. Substantial effects of hydrogen-bonded interactions between the channel and water on proton translocation were found. Smondyrev and Voth[16] used the multistate empirical valence bond model to describe interactions between the solvated proton and the environment of the influenza A virus M2 channel. Their MD simulations revealed that the excess proton was able to transport through the ring of histidine residues by hopping between water molecules. Therefore, the proton diffusion in the channel may be correlated with the changes in channel conformations.

In this work, we apply quantum chemical approaches to characterize stages of the proton shuttle along the chain of water molecules attached to molecular walls, which mimic the polypeptide environment of ion channels. Keeping in mind future applications of these theoretical tools for studies of the proton transfer in the M2 channel of influenza A virus,[16−22] we consider the models which have some relevance to the molecular configuration of this membrane protein. According to the working hypothesis of the proton transport and gating in M2, [17] the proton transfer occurs along the network of water molecules that fills the pore of the channel, interrupted by the histidine (His) residues, located approximately at the center of the bundle of four peptide helices of the protein. The destination point of the proton move may be assigned to the aspartic (Asp) residues at the intracellular ends of the helices. It is believed that a histidine residue is directly involved in the process of proton transfer across the M2 channel.[17,20,22] This is illustrated in Figure 1, which is drawn following the sketch from the article of Schweighofer and Pohorille. [22] In the initial state, an ϵ-protonated histidine accepts a proton through surrounding water molecules on the unprotonated N_δ atom of the imidazole ring. A positively charged intermediate with both protonated N_ϵ- and N_δ-atoms can relax by eliminating proton from the N_ϵ center, thus shuttling the proton to the water chain. It is believed that this model is consistent with the experimentally observed

* To whom correspondence should be addressed. E-mail: anem@lcc.chem.msu.ru (A. V. Nemukhin); topol@ncifcrf.gov (I. A. Topol).

† M.V. Lomonosov Moscow State University.

‡ National Cancer Institute at Frederick.

10.1021/jp027283x CCC: $25.00
Published on Web 03/07/2003

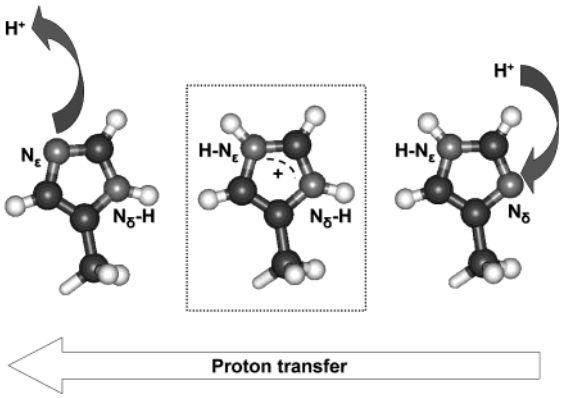

Figure 1. Illustration of the proton shuttle mechanism mediated by the His residue.[22]

proton selectivity as well as the pH dependence of the M2 channel conductance. [17]

In this work, we primarily focus on a separate stage of the process referring to the proton transfer from the biprotonated His to the Asp residue through water molecules. Because the proton affinity of the oxygen atom in the Asp CO_2^- group is higher than that of the imidazole nitrogen, the system with an excess proton located on His presents a local minimum on the potential energy surface, whereas the system with a proton residing on Asp (that is the end of the proton transfer path) presents the global minimum. Therefore, we can specify a perfect driving force for a proton movement from His to Asp through several water molecules, presumably through the well-defined transition state (TS). When we began our simulations, we did not know whether there would be a single TS on the reaction energy profile or a series of TSs. According to the MD studies for proton wires cited above, creation of transient structures with a proton captured by two or three water molecules is a likely event in the wire, and therefore, one can expect several local minima occurring on the energy profile.

First, we considered a single helix from the 4-fold bundle in which His and Asp residues were placed in their proper positions, and all other residues were replaced by glycines. Seven water molecules were added to the system. A treatment of this model was carried out by using a newly developed[23,24] version of the QM/MM method [11] based on the effective fragment potential theory. [25] The QM/MM boundary extended over the $C_\alpha-C_\beta$ bonds of His and Asp residues, and the polyglycine tube was treated as the MM subsystem. By using a series of geometry optimizations, we found equilibrium configurations for the systems with deprotonated and protonated states of His and Asp and estimated an energy barrier required for the proton detachment from His to the neighboring water molecule on the way to Asp.

To specify the intrinsic reaction coordinate (IRC) energy profiles for the proton transfer by using ab initio quantum chemistry methods, we have considered simplified models which mimic water wires attached to molecular walls containing His and Asp basic units. For these model systems, the customary quantum chemistry methods (Hartree−Fock, MP2, and B3LYP) were applied which allowed us to compute complete nonempirical energy profiles for the proton transfers from His to Asp through water wires. The results of these calculations also allowed us to evaluate the reliability and accuracy of lower level methods used in simulations of more extended systems.

Section 2 of the paper is devoted to a detailed description of molecular models used in simulations as well as of computational methods. In Section 3, we collect the results of calculations. Section 4 presents the main conclusions and discussion.

2. Models and Computational Details

We consider several molecular models related to the problem of the proton transfer along the water wires attached to the molecular systems containing His and Asp residues. There are two basic requirements for such models. First, we should consider the most important reactions of cleavage and formation of chemical bonds in proton wires at the ab initio quantum mechanical level. Second, a water wire should be attached to a fairly rigid molecular wall in order to mimic the conditions of protein tubes in ion channels.

The most extended molecular model is investigated here with the help of a new realization[23,24] of the QM/MM method,[11] which provides an excellent opportunity to meet these requirements. In brief, in this QM/MM approach, we exploit advantages of the effective fragment potential (EFP) technique[25] to take into account polarization of the electron density of the quantum subsystem due to effects of the MM part and to create a smooth interface between the QM and MM subsystems. The MM part, representing in this work a polypeptide helix, is considered as a flexible chain of small effective fragments (CONH, CH_2, CH, and CH_3). Each such fragment interacts with the QM part as prescribed by the original EFP-based QM/MM theory, [25] but the EFP−EFP interactions are replaced by the MM force fields. Therefore, in our QM/MM scheme, all atoms of QM interact with all atoms of MM, and polarization effects from the environment are fully taken into account. In practice, a combined use of the quantum chemical package GAMESS[26] (or its version PC GAMESS[27]) with the molecular modeling system TINKER[28] performs the QM/MM calculations. The computer program permits the user to select which MM fragments remain their positions fixed and which fragments are allowed to move during geometry optimization of the system.

Initial coordinates for the model system (model A for future references) were taken from the structure for the M2 ion channel obtained by the results of computer modeling consistent with the NMR and CD experimental studies.[22] A single strand was selected, and all of the residues beyond Asp and His were replaced by glycine units. Geometry configuration of the system was preliminary optimized at the molecular mechanical level by using the TINKER program [28] with the OPLS-AA [29] set of parameters. The QM/MM boundary was introduced over the $C_\alpha-C_\beta$ bonds of His and Asp residues saturating the valences by the link hydrogen atoms. The remaining part of the helix constituting the MM subsystem was partitioned into 43 small effective fragments. The approximate total length of the helix was 27 Å. Five water molecules filled the space between the N terminus of the sequence and His. Two of them, closest to His, were included into the QM part, whereas the remaining three water molecules were described by effective fragment potentials with the library parameters contained in GAMESS. [26] We only replaced EFP−EFP interactions between these water effective fragments by the conventional TIP3P parameters. Two water molecules belonging to the QM part were introduced between Asp and His.

Figure 2 illustrates the entire system for the QM/MM calculations for model A. The atoms of the QM part are shown in the ball-and-stick representation. The MM composition of effective fragments, positions of which are fixed in geometry optimizations, is shown in lines. The effective fragments closest to the QM/MM boundary, as well as three EFP water molecules (shown in sticks), were allowed to move in optimizations.

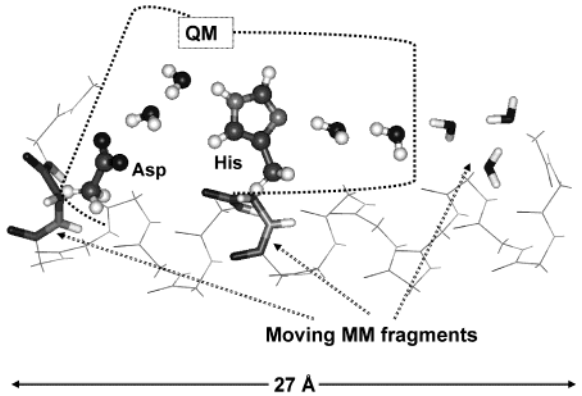

Figure 2. Model molecular system for QM/MM calculations (model A). Ball-and-stick representation is used for the atoms included into the QM subsystem, which is circled around by a dotted line. The part of the polyglycine tube shown in lines consists of MM effective fragments, positions of which have been fixed. The fragments shown in sticks, including three water molecules, have been included in the geometry optimization.

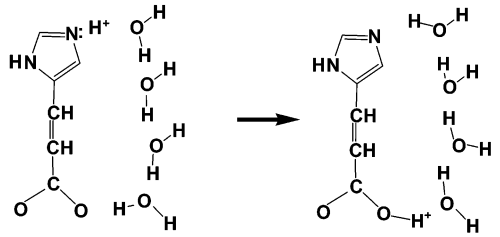

Figure 3. Scheme of a proton transfer in the model molecular system with a four member water wire (model B).

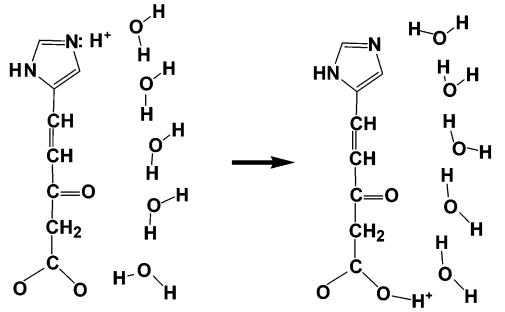

Figure 4. Scheme of a proton transfer in the model molecular system with a five member water wire (model C).

The QM calculations were carried out at the restricted Hartree−Fock (RHF) level with the 6-31G basis set. The OPLS-AA set of parameters was employed in the MM calculations.

Simulations for the smaller molecular models have been performed at the ab initio levels by assigning all atoms to the quantum part. Figure 3 illustrates the scheme of transformations occurring in the system with a four member water wire attached to the wall, which mimics a His−connect−Asp molecular fragment. To provide a proper rigidity to the wall, we introduce the connector −HC═CH− between the functional groups. The left and right sides of Figure 3 show the system at the beginning and at the end of the process of proton transfer over the chain of water molecules. As it was found, both geometry configurations correspond to the true minima on the potential energy surface, the right one being lower in energy. We shall refer to this system as to model B.

The next system (model C) shown schematically in Figure 4 contains one more water molecule in the wire giving rise to a pentamer and also differs from the previous system in an important respect. Namely, the wall includes the functional group −C═O which can interact with a nearby water molecule much stronger than the hydrophobic groups of the previous model (Figure 3).

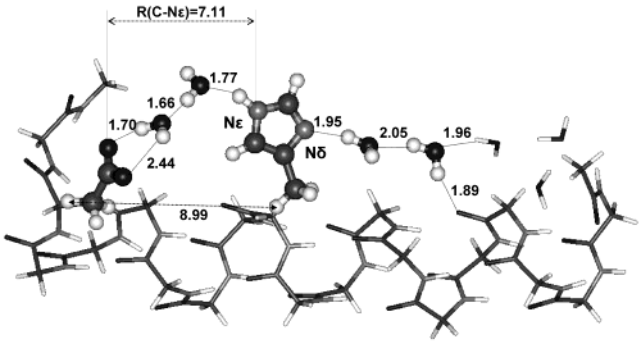

Figure 5. Model A: Equilibrium geometry configuration in the initial state with the unprotonated histidine. Distances are given in Å.

For the models B and C illustrated in Figures 3 and 4, we were able to locate true transition states for the proton transfer from the N_ϵ atom of imidazole to the neighboring water molecule and to construct the intrinsic reaction coordinate (IRC) paths starting from the saddle points. The majority of calculations were performed at the Hartree−Fock level by using the Stevens−Bash−Krauss pseudopotentials and the corresponding basis sets.[30] PC GAMESS program package[27] was employed in simulations.

Because in all previous models A−C we utilized the Hartree−Fock approximation for quantum calculations, we needed to evaluate the importance of electron correlation effects to achieve quantitative conclusions. To this goal, the smallest model D was constructed which included the imidazole ring directly bound to the CO_2^- group and the wire of three water molecules with an excess proton. For this model, the transition state configurations were found and the IRC energy profiles were computed in the Hartree−Fock approximation with different basis sets as well as at the B3LYP/6-31+G(d,p) and MP2/6-31+G(d,p) levels using the Gaussian 98 program. [31]

3. Results

Model A. In Figure 5, we show the result of QM/MM geometry optimization for the system with a neutral (unprotonated) His residue.

One can see a perfect network of hydrogen bonds extending from the water molecules at the channel entrance up to Asp, directly including nitrogen atoms of His. Beyond hydrogen bond lengths, we show the distance between link hydrogen atoms on the QM/MM boundaries (we remind the reader that positions of the effective fragments of the MM chain in the immediate vicinity of the QM part are optimized) and the distance between the carbon atom of the CO_2 group and the N_ϵ atom of the imidazole ring. The latter distances turn out to be very sensitive to the protonation state of Asp and His. It is worth noting formation of hydrogen bonds between water molecules to the right from His and the carbonyl groups of the peptide tube. One such bond of length 1.89 Å is explicitly specified in Figure 5. Three water molecules described by EFPs are also involved into the hydrogen bonding networks.

When an excess proton was added to the system in such a manner that the H_3O^+ ion was created, instead of any of two water molecules to the right from His, the geometry optimization procedure resulted in an equilibrium structure with the biprotonated His product shown in Figure 6. No other minimum

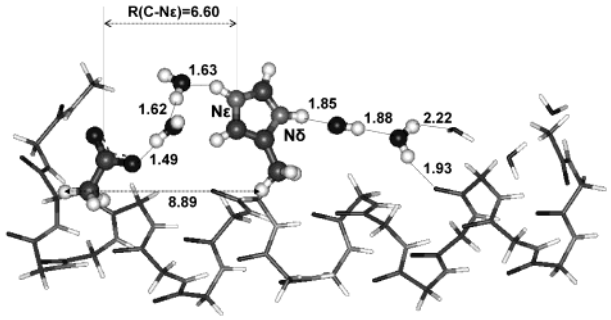

Figure 6. Model A: Equilibrium geometry configuration for the biprotonated histidine. Distances are given in Å.

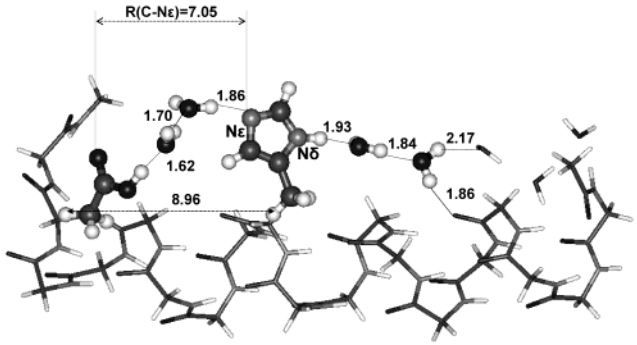

Figure 7. Model A: Equilibrium geometry configuration of the system with protonated Asp at the destination point of the proton transfer. Distances are given in Å.

energy configurations corresponding to either H_3O^+ or $H_5O_2^+$ units in the hydrogen bond networks were found.

As expected, protonation of the His residue resulted in drastic changes in the hydrogen bond network compared to the case of unprotonated His. The arrangement of water molecules around His is now totally different. Because of a strong Coulombic attraction, the Asp and His fragments are getting much closer: the distance between C of the CO_2 group and N_ϵ of the imidazole ring is reduced by 0.5 Å, and even the distance between the link atoms is reduced by 0.1 Å.

The final stage of the proton transfer to Asp requires the cleavage of the $N_\epsilon-H$ bond, and when that happens, a wire over two water molecules is created resulting in protonation of Asp. The corresponding minimum energy configuration is shown in Figure 7. We note that, as the $N_\epsilon-H$ bond was stretched to a certain threshold (see below), the geometry optimization procedure smoothly followed directly to the global minimum with the protonated Asp without any indication of local minima in between.

Similarly to the step of protonation of His, a noticeable rearrangement of water molecules occurs accompanying a proton transfer from His to Asp, and the initial separation between Asp and His is restored (compare Figures 5 and 7).

In Figure 8, we summarize the geometry changes during the proton-transfer cycle by showing the equilibrium geometry configurations of the system from another perspective. The panels of Figure 8 can be compared to the corresponding panels of Figure 1, illustrating, schematically, the proton shuttle mechanism with a direct involvement of histidine.

In Figure 8, for clarity, we deleted the terminal parts of the helix and also the water molecules that are not involved in the wire connecting His and Asp. What is clearly seen from this view is that His remains approximately in the same orientation with respect to the helical tube, whereas Asp fluctuates considerably during the changes in protonation state of His and

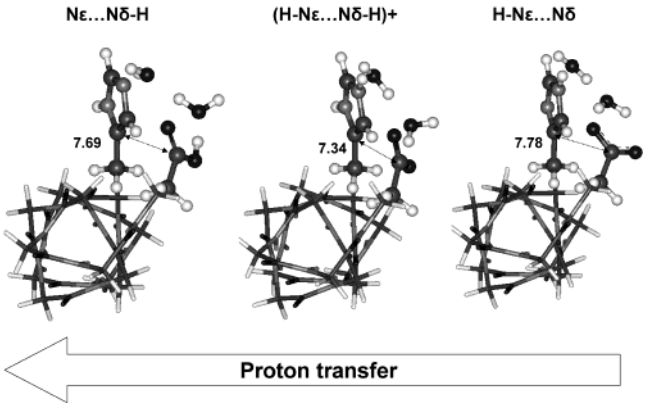

Figure 8. Model A: Equilibrium geometry configurations of the system during the proton-transfer cycle. Right, the initial structure with the unprotonated His; center, biprotonated His; left, protonated Asp. Distances between the C_γ atoms of His and Asp are given in Å.

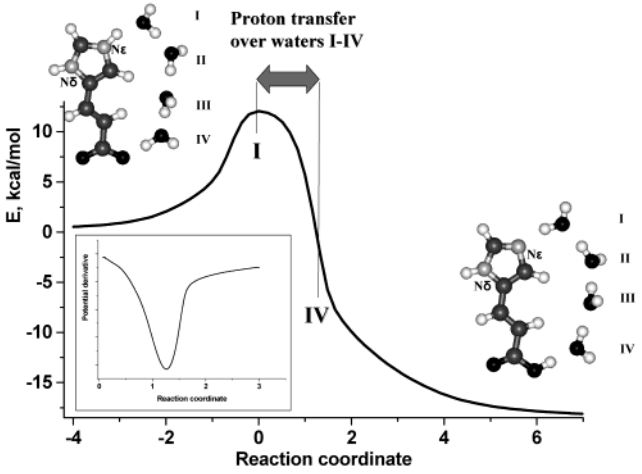

Figure 9. Model B: The steepest descent path for the proton transfer along water tetramer. The marks I and IV indicate approximate positions, where the hopping proton leaves the first and fourth water molecules, counting them from the top in the pictures. The inset shows the graph of the first derivative of this potential, the minimum of which almost coincides with point IV on the main graph.

Asp. In Figure 8, we plot the distances between C_γ atoms of His and Asp. We also estimated the dihedral angle between planes of the imidazole ring of His and the CO_2 group of Asp and found that it varied within 50° when protonation of His took place.

By using a series of constrained geometry optimizations, we estimated the energy barrier height for the proton detachment from the N_ϵ atom of the biprotonated His residue. Starting from the structure shown in Figure 6, we consequently stretched the $N_\epsilon-H$ bond from the initial equilibrium value of 1.03 Å and performed optimization of all other geometry parameters by keeping the corresponding $N_\epsilon-H$ bond length fixed. We found that for $N_\epsilon-H$ distances greater than 1.26 Å the water wire was initiated, resulting in final protonation of Asp. The energy increase compared to the point of the local minimum of the biprotonated state of His was found to be 5.8 kcal/mol.

Model B. By using the RHF/SBK calculations, we were able to locate the stationary points (global and local minima and TS) for the model system illustrated in Figure 3. The results of calculations are presented in Figure 9 where we show the computed energy profile for the proton-transfer reaction. The points on the *X* axis, presenting reaction coordinates (the mass weighted coordinates), are given in atomic units.

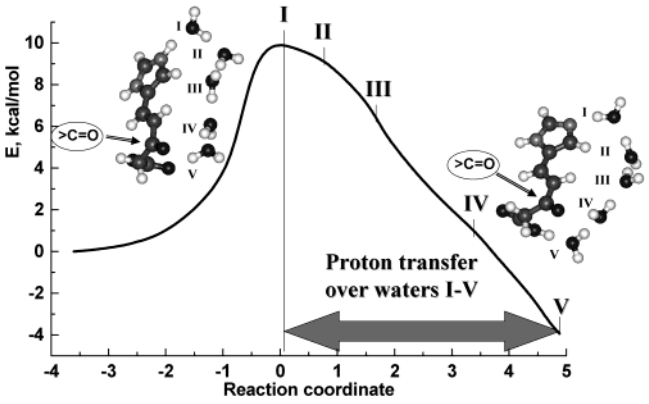

Figure 10. Model C: The steepest descent path for the proton transfer along water pentamer.

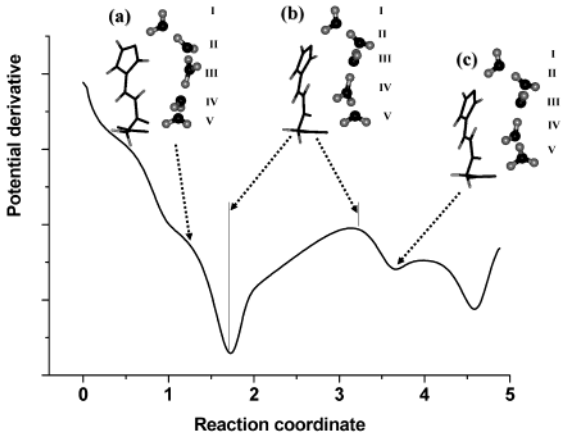

Figure 11. Model C: The graph of the first derivative of the potential of Figure 10 for the proton transfer over 5 water molecules. The insets a, b, and c show configurations of the system in the positions indicated by arrows.

The molecular systems shown in the panels of Figure 9 for the initial (left) and final (right) stages correspond to the true minima on the potential surface, the final system being 18.7 kcal/mol lower in energy at the SCF/SBK level. The activation barrier for the starting step to remove the proton from the wall is estimated as 11.9 kcal/mol. Remarkably, the computed profile to the right from the saddle point is completely barrierless. Obviously, the groups of atoms in the water wire readily adjust their positions, following the steepest descent path, when the units H_3O^+ are formed in the wire. In the graph shown in the inset of Figure 9, one can see that at the position of the inflection point of the potential energy curve its first derivative has a deep minimum.

It is instructive to apply the natural bond orbital (NBO) analysis[32] in order to recognize at every point along the reaction path the status of the wire and determine the positions where the H_3O^+ units are located. In particular, we can conclude that at the point, marked by a symbol IV in the energy graph, the excess proton already has left the water wire and belongs to the molecular system assigned to the wall (the right panel in Figure 9). Also according to the NBO analysis, in the regions to the left from the point, marked by I, the proton may be assigned to the first water molecule (counting from the top in the chain), whereas in the regions to the right from this point, the H_3O^+ unit is the neighboring species (the second from the top). Therefore, we can estimate a total way for the proton transfer over the water tetramer in this system as a region between points I and IV.

Model C. An even more interesting picture emerges for model system C (Figure 4), which was also studied using the RHF/SBK method. In this model, the molecular wall includes the hydrophilic functional group −C═O, which can form hydrogen bonds with water molecules in the wire. We see evidences of such interactions in Figures 5−7. The most important section of the reaction path over the water pentamer, obtained in the same manner as the previous case of model B, is illustrated in Figure 10. Similarly to the previous case, the energy profile for proton transfer over the chain of water molecules shows the only maximum corresponding to the transition state for proton detachment from the N_ϵ atom of imidazole. The computed energy barrier, 9.8 kcal/mol, is about 2 kcal/mol lower than for model B.

As for the model B, we analyze the graph of the potential derivative for the fraction of reaction path to the right from the saddle point (Figure 11).

When performing the NBO analysis for a variety of points along this curve, we can indicate the approximate positions of the changes in the state of the wire. The point marked by I separates the regions in which the excess proton belongs to the first and the second water molecules (counting from the top in the pictures of Figures 10 and 11). The point II separates the regions of the proton transfer between the second and third water molecules and so forth. To the right of point V, the proton returns to the wall and attaches to the CO_2^- group.

Similarly to the previous case of the water tetramer in model B, a point where the proton leaves the wire can be recognized by analyzing the graph of the first derivative of the potential (Figure 11): this is a position of the farthest (to the right) minimum of the derivative. Other features in the derivative curve are also interesting. The deepest minimum (the point of lowest speed) is located at approximately $^1/_3$ of the reaction path. To the left of this point, the H_3O^+ unit is in the center of the wire, as shown by panel a. Then, the proton is transferred to the fourth (from the top) water molecule and stays with this species for a long time: at the position of a local maximum nearest to the deepest minimum of the derivative, the H_3O^+ unit is still the fourth species (panel b). After that, the transfer to the neighboring fifth water molecule is accomplished, as shown by panel c.

Clearly, the reason for such lengthening of the proton-transfer reaction way is the occurrence of the hydrophilic −C═O group closely in space to the fourth water molecule in the wire. Strong hydrogen bond interactions with this functional group prevent the corresponding species in the wire from readily adjusting their positions.

An important conclusion can be drawn from the analysis of energy profiles for the proton transfer over the chain of water molecules in the presence and in the absence of a molecular wall to which the wire is attached.

We compare in Figure 12 the potentials for a pentamer wire taken from model C, which have been obtained within two approaches. The curve with circles reproduces the most important section of the entire reaction path of Figure 10, but the origin of energy is shifted if we consider the value at the TS as zero. The energy gradually decreases while the proton moves along the water chain attached to the wall. The second graph in Figure 12 marked by asterisks is computed as follows. We take geometry configurations of the subsystem $H^+(H_2O)_5$, precisely as those as obtained in calculations of the steepest descent path in the presence of molecular wall, and recompute energies of the wire without the wall. The picture of this graph clearly shows a qualitatively different behavior of the potential. An obvious minimum corresponds to the wire with a position of the H_3O^+ unit in the center, and the energy grows rapidly

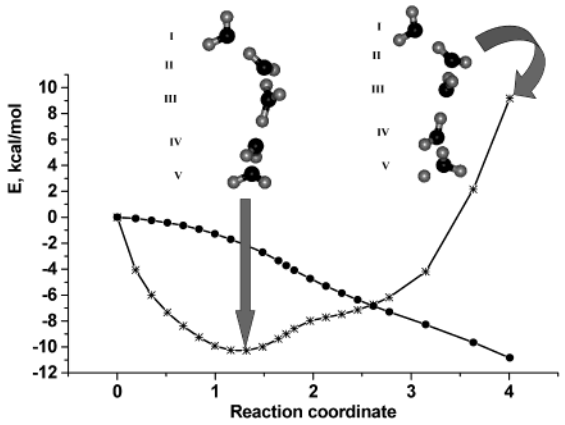

Figure 12. Model C: Potentials of the proton transfer over five water molecules. The curve with circles presents the section of the path shown in Figure 10 between points I and V for the entire model molecular system. The curve with asterisks illustrates the results of calculations for the subsystem $H^+(H_2O)_5$ in exactly the same geometry configurations but in the absence of the molecular wall.

upon translocation of the proton to the end of the wire. We do not present here the results of similar calculations for the water tetramer (model B), which lead to the same picture. According to these calculations, the simulations of the proton transfer for the wires, which are assumed to be in a vacuum, although under constraints of cylindrical symmetry, should not give an adequate representation of potential energy surfaces of proton wires in ion channels.

Model D. Figure 13 summarizes the main results obtained for the smallest molecular model considered in this work but using several quantum chemical approaches. In model D, the imidazole ring originating from His and the CO_2^- group from Asp are directly bound by an ordinary chemical bond. We computed equilibrium geometry parameters for the point of the local minimum (left panel in Figure 13), corresponding to the biprotonated state of His, for the global minimum (right panel), corresponding to the final state of the proton transfer, and for the saddle point (central panel).

TABLE 1: Heights of the Energy Barrier for Proton Detachment from the ϵ-Nitrogen Atom of His Calculated in Different Molecular Models

model	calculation method	energy, kcal/mol
A	QM(RHF/6-31G)/MM(OPLS-AA)	5.8
B	RHF/SBK	11.9
C	RHF/SBK	9.8
D	RHF/SBK	15.1
	MP2/6-31+G(d,p)	14.2
	B3LYP/6-31+G(d,p)	12.4

The results of the RHF/SBK approximation, used also for models B and C, are shown at the top of each column referring either to a equilibrium geometry parameter or to the relative energy. The middle values in the columns refer to the MP2/6-31+G(d,p) approximation, and the values at the bottom are obtained with the help of the B3LYP/6-31+G(d,p) approach. Comparison of geometry configurations of these three stationary points indicates that the Hartree−Fock theory allows one to obtain fairly reasonable estimates of the optimized parameters. Comparison of the energy barriers for the proton detachment from the N_ϵ atom of the imidazole ring confirms a general rule, that the Hartree−Fock barriers are overestimated.

Concluding this section, we collect in Table 1 the calculation results for the single energy barrier found on the proton-transfer route for all models.

If we compare results of the Hartree−Fock approach, taking into account that the RHF/6-31G and RHF/SBK approximations are of comparable accuracy, then the computed barrier heights correlate with the complexity of the model, namely, the larger a molecular environment of the water wire, the smaller the barrier: 15.1 (D), 11.9 (B), 9.8 (C), and 5.8 (A). Comparison of the values obtained for model D at the Hartree−Fock and at correlation levels shows that the quantity 5.8 kcal/mol should be an upper limit for the most extended model A.

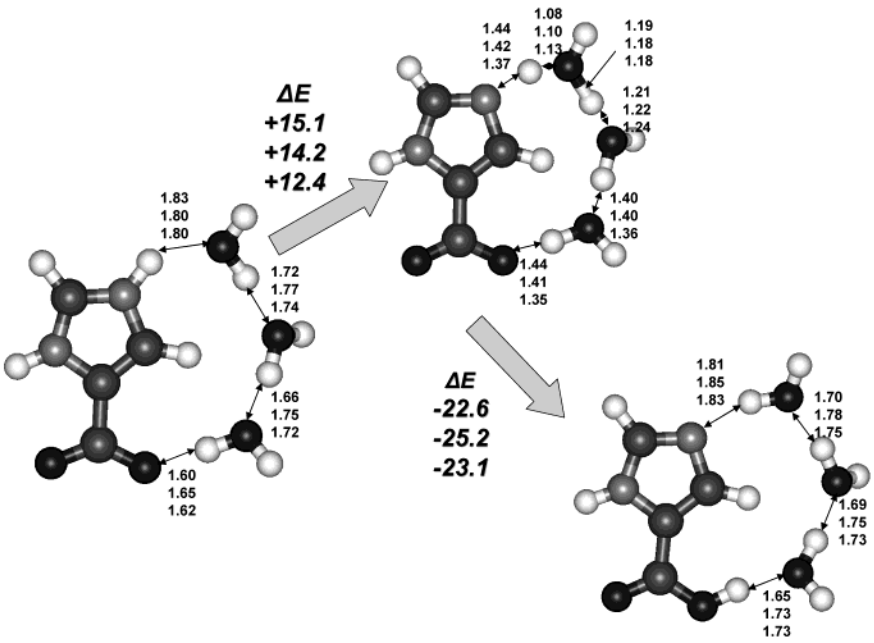

Figure 13. Calculation results for the model D. Left panel, the local minimum with a biprotonated imidazole ring. Central panel, the transition state for proton detachment from N_ϵ. Right panel, the global minimum as a result of the proton transfer over chain of three water molecules. The distances are given in Å. Energy differences ΔE between pairs of structures are given in kcal/mol. The ordering within each column is as follows: RHF/SBK calculation results (top), MP2/6-31+G(d,p) (middle), and B3LYP/6-31+G(d,p) (bottom).

4. Conclusions

Ab initio or QM/M calculations allow one to construct rigorous potential energy surfaces which can be helpful either for better calibration of the potentials to be applied in molecular dynamical (MD) calculations or for a combined use of quantum chemical and molecular mechanical forces in the MD routines. In this work, we used several quantum chemistry methods and considered several molecular models to study stages of the proton transfer processes in water wires attached to molecular walls containing the side chains of His and Asp residues. The driving force for the proton transfer over the chains of hydrogen bonded molecules can be principally specified by imposing some field along the molecular wall. In our modeling, this field is determined by the difference of proton affinities of His and Asp residues attached to hydrophobic walls. The most important steps of cleavage and formation of chemical bonds in proton wires are treated at the ab initio quantum mechanical level. The largest molecular model A is investigated with the help of a newly developed flexible effective fragment QM/MM method by using the Hartree−Fock theory for the quantum part. For the simplified molecular models B−D, the Hartree−Fock, MP2, and B3LYP techniques are applied. In all cases, we estimate or compute directly the minimum energy profiles for the proton transfer toward negatively charged molecular fragment presenting the Asp residue. Geometry configurations with the proton finally residing at Asp correspond to the global energy minimum of the molecular system. The only local minimum occurring in each system refers to the configurations with the biprotonated histidines. We found that no other intermediate structures (local minima) existed on the proton-transfer path, and the proton transfer along the molecular wall occurred barrierlessly. The energy required for detachment of another proton from the opposite side of the imidazole ring to continue the wire should not exceed 5 kcal/mol, which is a reasonable amount for the shuttle model. Calculations of the energy barrier for proton detachment from the biprotonated His with higher precision might be a subject of future studies.

It should be noted that this study does not pretend to explain mechanisms of proton translocations in biomolecular systems. More elaborate models are required to investigate proton transfer across chains of donors and acceptors in a proper environment. This subject is intensively covered, for example, in publications of the Warshel's group. [33,34] In the important paper of Sham, Muegge, and Warshel,[34] it is shown that processes of the proton transfer in proteins are controlled mainly by the electrostatic interaction between the proton site and its surroundings rather than by the local bond rearrangements of water molecules that are involved in the proton pathways. Effects of boundaries, for example, due to immersing the channel protein into water or membrane may also modify conclusions obtained in simulations without such constraints.

Another important aspect of this modeling is that we concentrate on the reaction pathways on the potential energy surfaces, whereas for proper dealing with biological systems, the free energy calculations are of a greater value. However, for the models discussed in this work, the barriers for energy should not differ substantially from the free energy differences.

Acknowledgment. We are grateful to Dr. R. Cachau for providing the molecular model of the M2 protein and for valuable suggestions during the study. We thank the reviewers of this paper for valuable comments and suggestions. The research described in this publication was made possible in part by Award No. RC1-2350-MO-02 of the U.S. Civilian Research and Development Foundation for the Independent States of Former Soviet Union (CRDF). This work is also supported in part by the grant from the Russian Foundation for Basic Researches (project 01-03-32071). We thank the staff and administration of the Advanced Biomedical Computing Center for their support of this project. This project has been funded in whole or in part with Federal funds from the National Cancer Institute, National Institutes of Health, under Contract No. NO1-CO-56000. The content of this publication does not necessarily reflect the views or policies of the Department of Health and Human Services, nor does mention of trade names, commercial products, or organization imply endorsement by the U.S. Government.

References and Notes

(1) Pomès, R.; Roux, B. *Biophys. J.* **1998**, *75*, 33.

(2) Sagnella, D. E.; Tuckerman, M. E. *J. Chem. Phys.* **1998**, *108*, 2073.

(3) Warshel, A. *Computer Modelling of Chemical Reactions in Enzymes and Solutions*; Wiley: New York, 1991.

(4) Åquist, J.; Warshel, A. *Chem. Rev.* **1993**, *93*, 2523.

(5) Vuillemier, R.; Bogris, D. *J. Phys. Chem.* **1998**, *102*, 4261. (b) Vuillemier, R.; Bogris, D. *J. Chem. Phys.* **1999**, *111*, 4251.

(6) Schmitt, U. W.; Voth, G. A. *J. Phys. Chem. B.* **1998**, *102*, 5547. (b) Schmitt, U. W.; Voth, G. A. *J. Chem. Phys.* **1999**, *111*, 9361.

(7) Brewer, M. L.; Schmitt, U. W.; Voth, G. A. *Biophys. J.* **2001**, *80*, 1691.

(8) Drukker, K.; de Leeuw, S.; Hammes-Schiffer, S. *J. Chem. Phys.* **1998**, *108*, 6799. (b) Decornez, H.; Drukker, K.; Hammes-Schiffer, S. *J. Phys. Chem. A.* **1999**, *103*, 2891.

(9) Mei, H. S.; Tuckerman, M. E.; Sagnella, D. E.; Klein, M. L. *J. Phys. Chem. B.* **1998**, *102*, 10446.

(10) Geissler, P. L.; Dellago, C.; Chandler, D.; Hutter, J.; Parrinello, M. *Science* **2001**, *291*, 2121.

(11) Warshel, A.; Levitt, M. *J. Mol. Biol.* **1976**, *103*, 227. (b) Singh, U. C.; Kollman, P. A. *J. Comput.Chem.* **1986**, *7*, 718. (c) Bash, P. A.; Field, M. J.; Karplus, M. *J. Am. Chem. Soc.* **1987**, *109*, 8092.

(12) Sadeghi, R. R.; Cheng, H.-P. *J. Chem. Phys.* **1999**, *111*, 2086.

(13) Meuwly, M.; Karplus, M. *J. Chem. Phys.* **2002**, *116*, 2572.

(14) Sagnella, D. E.; Laasonen, K.; Klein, M. L. *Biophys. J.* **1996**, *71*, 1172.

(15) Pomès, R.; Roux, B. *Biophys. J.* **2002**, *82*, 2304.

(16) Smondyrev, A. M.; Voth, G. A. *Biophys. J.* **2002**, *83*, 1987.

(17) Pinto, L. H.; Dieckmann, G. R.; Gandhi, C. S.; Parworth, C. G.; Braman, J.; Shaughnessy, M. A.; Lear, J. D.; Lamb, R. A.; DeGrado, W. F. *Proc. Natl. Acad. Sci. U.S.A.* **1997**, *94*, 11301.

(18) Sansom, M. S. P.; Kerr, I. D.; Smith, G. R.; Son, H. S. *Virology* **1997**, *233*, 163.

(19) Zhong, Q.; Husslein, T.; Moore, P. B.; Newns, D. M.; Pattnaik, P.; Klein, M. L. *FEBS Lett.* **1998**, *434*, 265.

(20) Mould, J. A.; Li, H.-C.; Dudlak, C. S.; Lear, J. D.; Pekosz, A.; Lamb, R. A.; Pinto, L. H. *J. Biol. Chem.* **2000**, *275*, 8592.

(21) Forrest, L. R.; Kukol, A.; Arkin, I. T.; Tielman, D. P.; Sansom, M. S. P. *Biophys. J.* **2000**, *78*, 55.

(22) Schweighofer, K. J.; Pohorille, A. *Biophys. J.* **2000**, *78*, 150.

(23) Nemukhin, A. V.; Grigorenko, B. L.; Bochenkova, A. V.; Topol, I. A.; Burt, S. K. *J. Mol. Struct. (THEOCHEM)* **2002**, *581*, 167.

(24) Grigorenko, B. L.; Nemukhin, A. V.; Topol, I. A.; Burt, S. K. *J. Phys. Chem. A.* **2002**, *106*, 10663.

(25) Gordon, M. S.; Freitag, M. A.; Bandyopadhyay, P.; Jensen, J. H.; Kairys, V.; Stevens, W. J. *J. Phys. Chem. A* **2001**, *105*, 293. (b) Wadkowski, B. D.; Krauss, M.; Stevens, W. J. *J. Am. Chem. Soc.* **1995**, *117*, 10537. (c) Day, P. N.; Jensen, J. H.; Gordon, M. S.; Webb, S. P.; Stevens, W. J.; Krauss, M.; Garmer, D.; Basch, H.; Cohen, D. *J. Chem. Phys.* **1996**, *105*, 1968. (d) Chen, W.; Gordon, M. S. *J. Chem. Phys.* **1996**, *105*, 11081. (e) Krauss, M.; Webb, S. P. *J. Chem. Phys.* **1997**, *107*, 5771. (f) Krauss, M.; Wadkowski, B. D. *Int. J. Quantum Chem.* **1998**, *69*, 11. (g) Roitberg, A. E.; Worthington, S. E.; Holden, M. J.; Mayhew, M. P.; Krauss, M. *J. Am. Chem. Soc.* **2000**, *122*, 7312. (h) Kairys, V.; Jensen, J. H. *J. Phys. Chem. A* **2000**, *104*, 6656. (i) Minikis, R. M.; Kairys, V.; Jensen, J. H. *J. Phys. Chem. A* **2001**, *105*, 3829. (j) Li, H.; Hains, A. V.; Everts, J. E.; Robertson, A. D.; Jensen, J. H. *J. Phys. Chem. B* **2002**, *106*, 3486.

(26) Schmidt, M. W.; Baldridge, K. K.; Boatz, J. A.; Elbert, S. T.; Gordon, M. S.; Jensen, J. H.; Koseki, S.; Matsunaga, N.; Nguyen, K. A.; Su, S. J.; Windus, T. L.; Dupuis, M.; Montgomery, J. A. *J. Comput. Chem.* **1993**, *14*, 1347.

(27) Granovsky, A. A. URL http://lcc.chem.msu.ru/gran/gamess/index.html.

(28) Ponder, J. W.; Richards, F. M. *J. Comput. Chem.* **1987**, *8*, 1016. (b) Kundrot, C. E.; Ponder, J. W.; Richards, F. M. *J. Comput. Chem.* **1991**, *12*, 402. (c) Dudek, M. J.; Ponder, J. W. *J. Comput. Chem.* **1995**, *16*, 791. (d) Hodsdon, M. E.; Ponder, J. W.; Cistola, D. P. *J. Mol. Biol.* **1996**, *264*, 585. (e) Kong, Y.; Ponder, J. W. *J. Chem. Phys.* **1997**, *107*, 481. (f) Dudek, M. J.; Ramnarayan, K.; Ponder, J. W. *J. Comput. Chem.* **1998**, *19*, 548. (g) Pappu, R. V.; Hart, R. K.; Ponder, J. W. *J. Phys. Chem. B.* **1998**, *102*, 9725. (h) URL http://dasher.wustl.edu/tinker.

(29) Jorgensen, W. L. In *Encyclopedia of Computational Chemistry*; Schleyer, P. v. R., Ed.; Wiley: New York, 1998; Vol. 3, p 1986.

(30) Stewens, W.; Basch, H.; Krauss, M. *J. Chem. Phys.* **1984**, *81*, 6026.

(31) Frisch, M. J.; Trucks, G. W.; Schlegel, H. B.; Scuseria, G. E.; Robb, M. A.; Cheeseman, J. R.; Zakrzewski, V. G.; Montgomery, J. A., Jr.; Stratmann, R. E.; Burant, J. C.; Dapprich, S.; Millam, J. M.; Daniels, A. D.; Kudin, K. N.; Strain, M. C.; Farkas, O.; Tomasi, J.; Barone, V.; Cossi, M.; Cammi, R.; Mennucci, B.; Pomelli, C.; Adamo, C.; Clifford, S.; Ochterski, J.; Petersson, G. A.; Ayala, P. Y.; Cui, Q.; Morokuma, K.; Malick, D. K.; Rabuck, A. D.; Raghavachari, K.; Foresman, J. B.; Cioslowski, J.; Ortiz, J. V.; Stefanov, B. B.; Liu, G.; Liashenko, A.; Piskorz, P.; Komaromi, I.; Gomperts, R.; Martin, R. L.; Fox, D. J.; Keith, T.; Al-Laham, M. A.; Peng, C. Y.; Nanayakkara, A.; Gonzalez, C.; Challacombe, M.; Gill, P. M. W.; Johnson, B. G.; Chen, W.; Wong, M. W.; Andres, J. L.; Head-Gordon, M.; Replogle, E. S.; Pople, J. A. *Gaussian 98*, revision A11.3; Gaussian, Inc.: Pittsburgh, PA, 1998.

(32) Reed, A. E.; Curtiss, L. A.; Weinhold, F. *Chem. Rev.* **1988**, *88*, 899.

(33) Warshel, A. *J. Phys. Chem.* **1979**, *83*, 1640. (b) Warshel, A. *J. Phys. Chem.* **1982**, *86*, 2218. (c) Warshel, A. *Proc. Natl. Acad. Sci.* **1984**, *81*, 444. (d) Warshel, A.; Chu, Z. T. *J. Chem. Phys.* 1990, *93*, 8682.

(34) Sham, Y. Y.; Muegge, I.; Warshel, A. *Proteins: Struct., Funct., Genet.* **1999**, *36*, 484.